https://doi.org/10.15407/ufm.23.03.489

M.B. BABANLI*, N.A. GURBANOV, and R.K. MEHTIYEV**
Azerbaijan State Oil and Industry University,
20 Azadlig Ave., AZ-1010 Baku, Azerbaijan

* mustafababanli@yahoo.com, **nurlan.gurbanov@asoiu.edu.az

FORMATION AND GROWTH OF CRACKS IN 7075-T6 ALUMINIUM MATRIX HYBRID FML NANOCOMPOSITE MATERIALS

The paper scopes on the experimental data, computer and theoretical (analytical) models of the crack formation processes in hybrid nanocrystalline materials with nanoparticle filler of 7075-T6 aluminium matrix under the influence of high-speed and quasi-static deformation regimes. Presenting the main experimental facts and results of the computer modelling, particular attention is paid to the theoretical models describing the formation of nanoscopic cracks in the tips of the microcracks in hybrid nanocrystalline materials at high speeds and quasi-static deformation. A model describing the formation and growth of nanocracks near the tips of the blunt cracks in a hybrid nanocomposite material is proposed. Within the model, the concentration of stresses at the tips of the blunt cracks causes the grain boundaries to slip and dislocations at the grain boundary junctions. The stresses, which create these dislocations, and the load applied to the crack peaks cause the nanocracks to form and grow. As shown, an increase in the radius of curvature at the tips of a thick crack and a decrease of the grains' size contribute to the growth of nanocracks. These trends are consistent with experimental data on the low decomposition viscosity and high plasticity of the most nanocrystalline materials.

Keywords: fibre metal laminate (FML), hybrid FML nanocomposite, elliptical crack, viscous collapse, tension, plasticity.

1. Introduction

The mechanical properties of nanocrystalline materials are determined by the small size of the grains and the high-volume fraction occupied by the grain boundaries, which restricts the movement of dislocations and activates new plastic deformation and disintegration mechanisms. In

Citation: M.B. Babanli, N.A Gurbanov, and R.K. Mehtiyev, Formation and Growth of Cracks in 7075-T6 Aluminium Matrix Hybrid FML Nanocomposite Materials, *Progress in Physics of Metals*, **23**, No. 3: 489–509 (2022)

particular, in nanocrystalline materials, the high-volume fraction of the grain boundaries, including the sliding of the grain boundaries [1, 2], the diffusion crawl along the grain boundaries [3, 4], and the stress bonds with the grain boundaries cause the deformation mechanisms to work. Thus, grain boundaries and their combinations play the role of the beginning and growth of the crack [5]. Studies of nanocrystalline materials [6, 7, 8] and computer simulations [9, 10] using electron microscopy during loading and the formation and growth of nanocrystalline metals in grain boundaries near the ends of blunt cracks at the junction of nanocracks [8, 11] have been identified. The formation of nanocracks in the joints of grain boundaries has been accepted as a result of the sliding of the grain boundary in deformable nanocrystalline materials that do not contain primary cracks [12, 13]. Nanocracks are thought to be formed from the stress field of the grain boundaries, the separation dipoles of the grain boundaries [12, 14–16] and the dislocation separation configurations [13] caused by the sliding of the grain boundaries. At the same time, models [12, 13] were considered without initial cracks in nanocrystalline materials. Numerous studies have shown that nanocracks are formed at the apex of the largest blunt cracks [6–8].

As a result of numerous literature studies, it was found that the formation and growth of macro and micro cracks in composite materials have been sufficiently studied. However, these problems have not been sufficiently studied in hybrid nanocomposite materials. In this study, 1 mm thick 7075-T6 Al sheet, one-way carbon fibre fabric and epoxy resin were used to produce hybrid fibre metal laminate (FML) composites according to 4/3 assembly procedure. Epoxy resin was used without additives in the first production. In the second production, 0.5% clay and 0.5% SiO_2 nanoparticles were added to the epoxy resin. The obtained composite samples were mechanically tested in accordance with ASTM standards. The study of the mechanical properties of 7075-T6 Al matrix hybrid nanocomposites with clay and SiO_2 nanoparticle fillers is characterized by unique mechanical properties, which are extremely interesting for high technology in a wide area. In particular, the hybrid composite material with nanocrystalline 7075-T6 Al matrix is characterized by very high strength and toughness values. In most cases, hybrid nanocrystalline materials with aluminium matrix have low plasticity and crack resistance, which significantly reduces the technological process. However, in recent years, several research groups have simultaneously produced hybrid composite materials with superplastic aluminium matrix with high strength and high plasticity characterized by low values of plastic deformation before collapse, or obtained at relatively low temperatures, high degrees of deformation. The high strength of hybrid nanocrystalline materials with different nanoparticle fillers

7075-T6 Al matrix and the nature of the combination of plasticity has been the subject of undisclosed and intense discussions.

One of the processes that characterizes the strength and plasticity of hybrid nanocrystalline materials with 7075-T6 aluminium matrix is the formation of cracks in such materials under mechanical loads. Therefore, in order to study the nature of the high (unique) mechanical properties of nanocrystalline metallic materials, it is extremely important to describe adequately the decomposition processes of nanocrystalline materials and to determine the mechanisms of nanocracks formation in such materials, taking into account their structural properties. This work deals with experimental and theoretical studying the formation of nanocracks near the vertices of blunt cracks in hybrid FML nanocomposite materials with 7075-T6 Al matrix in high degree and quasi-static deformation modes.

2. Materials, Theoretical and Experimental Methods

2.1. Materials

In this study, the following materials were used to produce 7075-T6 aluminium matrix hybrid FML nanocomposite reinforced with different nanoparticles. 7075-T6 Al sheets used as matrix material in hybrid FML composites were provided by the Manisha Steel Centre (Maharashtra, India) in the size of 22×22 cm^2 for the production of composite material and cut in the size of 10×10 cm^2. In the production of hybrid fibre metal laminate composites, MGS-L326 epoxy and its MGS-H265 hardener were used, as well as one-sided carbon fibre with a fibre density of 300 g/m^2. The 18 nm thick nanoclay (99.9% purity) and 15 nm thick silicon dioxide (99.50 purity) (SiO_2) were used as fillers in the production of hybrid FML composites.

2.2. Production Method of Nanoparticle Reinforced Hybrid FMLs

In this work, 1 mm thick 7075-T6 aluminium sheet and 2 layers of carbon fibre (CF) fabric reinforced according to the 4/3 assembly process (Al/CF 0°–CF 0°/Al/CF 0°–CF 0°/Al/CF 0°–CF 0°/Al) hybrid layered composite materials were produced. The carbon fibre fabric used in this composite material is one-way. The directions of the fibre are placed parallel to the direction of propagation of the aluminium sheets. The sequence and symbolic description of the produced composite is shown schematically in Fig. 1.

The materials assembled in the schematic sequence shown in Fig. 1 are pressed in a hot-pressing device at 120 °C and a pressure of 1 ton for 3 hours in a shielding gas medium. After 3 hours, the hybrid FML com-

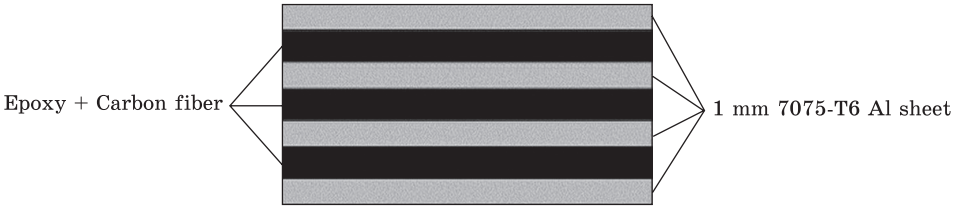

Fig. 1. Schematic description of the production process of hybrid FML nanocomposites

posite materials prepared in the hot-pressing device are removed from the device to cool at room temperature for 24 hours. Then, the required mechanical properties of hybrid FML composite materials are studied.

2.3. Theory and Computer Modelling of Hybrid FML Nanocry stalline Composite Materials under the Influence of High-Speed and Quasi-Static Deformations

In recent years, significant progress has been made in the experimental study of the structure and development of some hybrid nanocrystalline materials based on deformation, and high results have been achieved. However, due to the high demands on the accuracy of measurements, often at the atomic and nanoscopic levels, there are cases when modern experimental methods do not allow determining the characteristics of the hybrid nanocrystalline structure, the mechanism of deformation and fragmentation. In such situations, analytical theoretical models and computer modelling of the structure, plastic deformation and decomposition processes in this material are very important to understand the specific mechanical properties of hybrid nanocrystalline materials.

Analytical theoretical models of the structure and mechanical properties of hybrid nanocrystalline materials are based on analytical methods used in the theory of mechanical properties of traditional coarse-grained polycrystals and composites. The same is true of new theoretical concepts that take into account the properties of nanostructures and their effect on the processes of deformation and disintegration in nanocrystalline materials. In particular, the nanoscale theory of effective defect configurations is also used to describe changes in the nanocrystalline layers of solids during mechanical loading. According to this theory, defects are described as internal stress fields and plastic flux carriers that determine the deformation and disintegration processes of nanocrystalline materials at the nanoscale level.

In the theory of defects of nanocrystalline solids, the methods of the theory of elasticity are usually used. The limitations of analytical theoretical models are due to the natural method by which typical defective configurations and processes are studied. Atypical structures, defective configurations,

and processes are overviewed generally, although they can sometimes play an important role. In addition, analytical theoretical models are not always effective when describing structures and processes at different levels at the same time. Therefore, in order to confirm the results of analytical models, it is necessary to compare the experimental data with the results of atomic models.

Let us briefly discuss the general methodology, reliability, limitations and mechanical properties of computer modelling of nanocrystalline structures. In recent years, high results have been achieved in atomic modelling of deformation and disintegration mechanisms affecting nanocrystalline materials. These results are due to the sharp increase in the speed of computer computing in recent years and the development of parallel computing architecture. It turned out that the most effective method for atomic modelling of nanocrystalline solids in the process of plastic deformation is the method of molecular dynamics [17, 18].

This method has been used to simulate the relationship of different nanocrystalline structures under the influence of mechanical load at different times. This approach takes into account the anharmonicity of the crystal lattice and the very heterogeneous internal stresses in the deformable nanostructures. In addition to the attractive features of this approach, it has major drawbacks. That is, it is extremely short time frame that it is possible to simulate the behaviour of an atomic system in real time, and the reliability of the selected potential of interatomic interactions. As for the interactions between the atoms, they are described in terms of empirical interaction potentials. Their compatibility is generally checked when modelling flawless solids, when the nature of the electronic bond between the atoms and the complex changes close to the crystal lattice defects are not fully taken into account. In addition, most atomic models are designed for monoatomic nanostructured solids. Their application for the analysis of the development of polyhydric and composite nanostructures is limited by the difficulty of accurately describing the interatomic potentials of two or more atomic types. As a result, the results of computer simulation of deformation processes in nanocrystalline structures are applied directly to high-degree deformation. However, modelling the molecular dynamics of the plastic deformation of nanocrystalline materials provides important information about the structural transformations, which occur in nanocrystalline solids.

2.4. Viscous and Brittle Decomposition Processes in Nanocrystalline Materials

Tensile testing. Tensile testing was performed in accordance with ASTM D3039/D3039M-17 to determine the mechanical properties of hybrid FML nanocomposites. Tensile testing of FML nanocomposites was carried out on a MTS 100 kN traction tester at a pulling speed of 1 mm/min^{-1}.

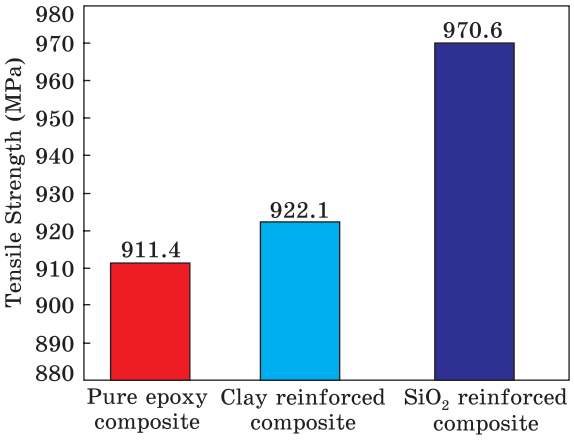

Fig. 2. Results of tensile testing of hybrid FML composites [8, 20]

Impact testing. In this study, Charpy impact test was performed at room temperature in accordance with ASTM E23 to determine the impact viscosity of hybrid FML nanocomposites. According to the composition of hybrid FML composites, samples of 55× × 10 mm^2 were prepared for each composite. Impact viscosity was measured on a ZWICK 450 J impact tester. Impact viscosity was applied to the samples in two different straight and lateral directions.

Optical analysis. A Nikon shuttle pics portable digital stereo microscope was used to investigate the interface characteristics of hybrid FML composite materials and samples after mechanical tests applied to these materials.

The results of the tensile testing of hybrid FML composite materials according to ASTM D3039/D3039M-17 are given graphically in Fig. 2 [8, 19, 20]. According to the graph, the tensile resistance of the hybrid FML composite produced with pure epoxy is 911.4 MPa. The tensile strength of hybrid FML nanocomposite produced with epoxy with the addition of 0.5% clay nanoparticles increased by 927.1 MPa and the tensile strength increased by 1.17% compared to composite materials produced with pure epoxy. The tensile resistance of the hybrid FML nanocomposite produced with 0.5% SiO_2 epoxy is 970.6 MPa. Compared to pure epoxy composites, the tensile strength of these hybrid FML nanocomposite materials is increased by 6.49%.

The impact viscosity of FML composites can be defined as the ability of materials to absorb impact energy when subjected to impact loading until deformation or collapse occurs. Compared to metal alloys, which absorb energy through elastic–plastic deformation, FML is observed in the structure of composites with different breaking mechanisms such as fibre splitting and fibre breakage to absorb mixed nuclear shock energy [21].

To determine the impact behaviour of hybrid FML composites against any impact, these composite materials were subjected to a Charpy impact test at a speed of 5.23 m/s according to the ASTM E23 standard. During this test, forces were applied to the hybrid FML composite samples in two different directions, straight and lateral, and the results were plotted in Fig. 3 [20].

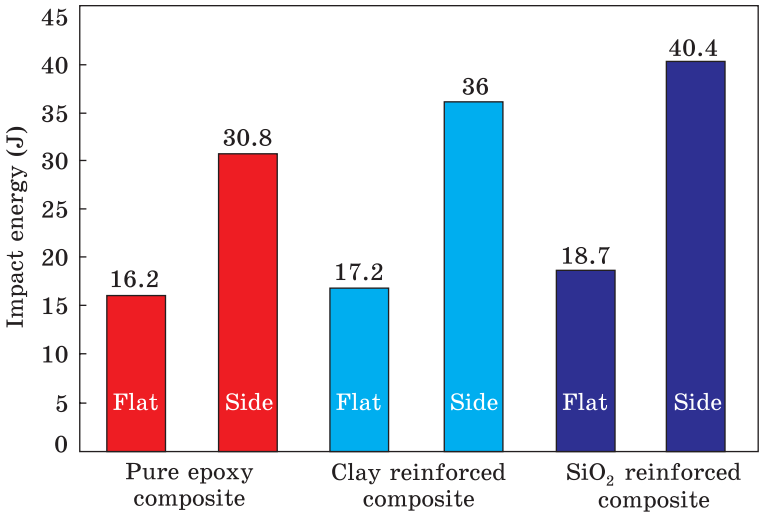

Fig. 3. Impact test results of hybrid FML composites [20]

As a result of the impact test of hybrid FML nanocomposites in accordance with ASTM E23 standards, the highest impact energy was observed in hybrid FML composites reinforced with 0.5% SiO_2 nanoparticles with a value of 18.7 J (flat), 40.4 J (side). The addition of 0.5% clay increased the impact energy of hybrid FML nanocomposites by 17% compared to FML composites produced with pure epoxy in the lateral direction. According to the graph, FML composites reinforced with 0.5% SiO_2 nanoparticles showed a 31% increase in lateral impact energy compared to pure epoxy composites.

The presence of a large number of boundary phases in nanocrystalline materials has a significant effect on the decomposition processes (Fig. 4). Grain boundaries are the preferred location for the formation and growth of nanocracks due to the low atomic density and weak interatomic bonds at such boundaries compared to the crystal structure inside the grains. In the presence of viscous disintegration in microporous compounds, the grain boundaries accelerate the diffusion-controlled growth of micropores with high diffusion permeability. In addition, the energy of the grain boundary phase contributes to the disintegration driving force, because as the grains grow along the boundaries, the cracks essentially disappear. At the

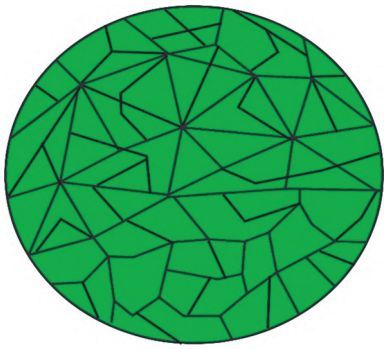

Fig. 4. Grain boundaries of hybrid FML nanocrystalline solids

same time, in nanocrystalline materials, the grain boundaries are generally short and curved in numerous compounds. Therefore, in a situation where cracks along the grain boundaries tend to grow, the complex geometry of such boundaries has a negative effect on the intergranular fracture processes.

In nanocrystalline materials, which are characterized by a high density of grain boundaries, there is competition between intra-grain and inter-grain decomposition processes. Depending on the structural parameters of the material and the loading conditions, one of these processes is preferred. Mechanically loaded nanocrystals persist simultaneously in a solid, and in addition to grain size, other factors affect the decomposition processes of nanocrystalline metals. In particular, the presence of microcracks, pores, defects in the material contributes to the formation of cracks and their growth.

3. Formation of Nanocracks at the Junctions of Grain Boundaries in the Nanocrystalline Materials

Forty times magnified microstructures of hybrid FML composite materials produced in accordance with the 4/3 stacking sequence are shown in Fig. 5 [20]. When the microstructures are examined in general, the lamination process between the metal and composite layers appears to be successful (Fig. 6).

The positive effect of nanoparticles on mechanical properties was determined in experiments. The addition of clay and SiO_2 nanoparticles to the epoxy resin appears to improve the adhesion properties between the boards in hybrid FML composites and has a positive effect on lamination.

The data of experimental studies of the microstructure of mechanically loaded nanocrystalline materials are of great importance for understanding the characteristic regularities and identifying typical micromechanisms of their disintegration. The experimental data discussed [22, 23] and the results of computer modelling [24] show the special role of compounds in the formation of preferred nanocracks in nanocrystalline materials. In the nanocrystalline materials, which are a very large part of the boundary compounds, nanocracks in such compounds may be typical elementary decay carriers. In this context, the mechanism of formation of nanocracks in FML nanocomposite compounds is of great interest.

Consider a nanocrystalline solid consisting of nanoparticles with a long blunt crack and grain boundaries separating them (see Fig. 7, *a*). Suppose that a nanocrystalline solid is subjected to a uniform tensile load. The cross-section of a typical fragment of a nanocrystalline solid is shown in Fig. 7, *a*, and the crack intersects the grain boundary at a distance from the nearest junction (Fig. 7 [25]).

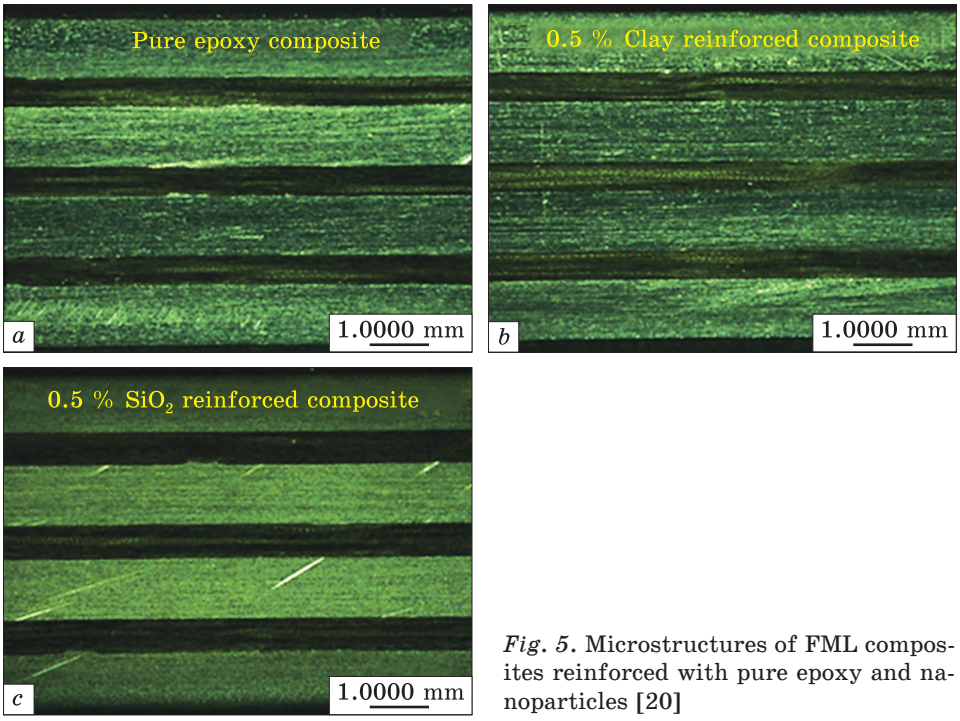

Fig. 5. Microstructures of FML composites reinforced with pure epoxy and nanoparticles [20]

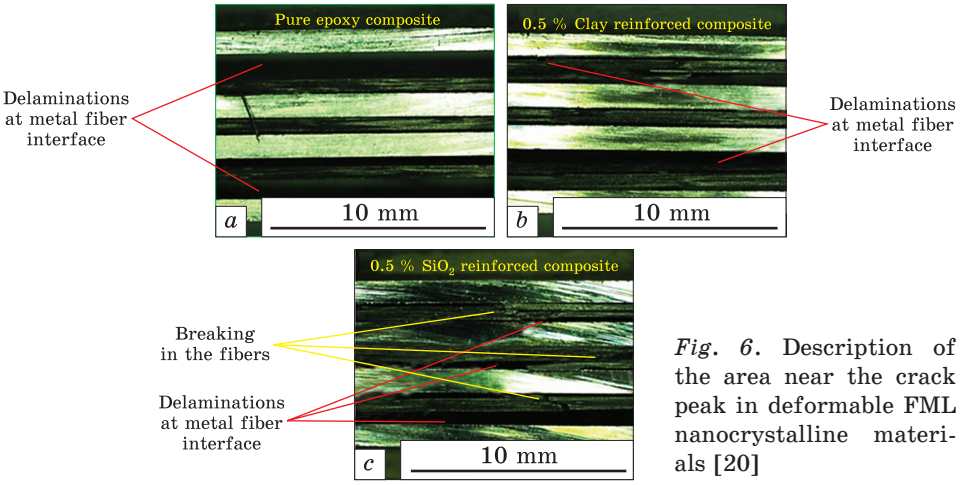

Fig. 6. Description of the area near the crack peak in deformable FML nanocrystalline materials [20]

The stresses acting on the crack peak in the deformed body cause the grain boundaries to slip along *AB* (Fig. 7, *b*) and other grain boundaries near the end of the crack. In this case, the combination of *B* prevents the grain boundary from sliding along the *AB* grain boundary, resulting in the grain boundary slip causing incomplete plastic displacement near this joint. From the point of view of the theory of defects of solids,

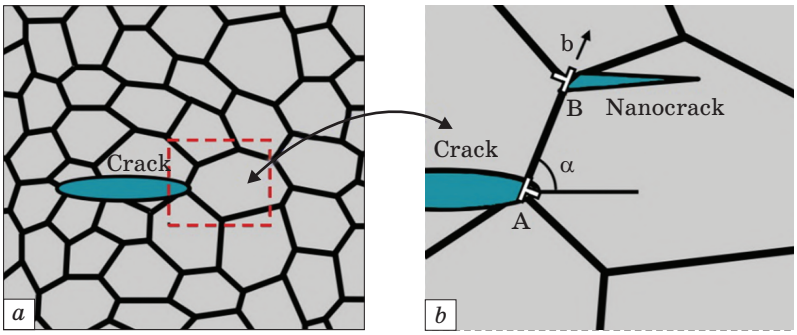

Fig. 7. Elliptical crack in deformable FML nanocrystalline materials: (*a*) general view, (*b*) sliding of the grain boundary along the *AB* boundary near the top of the long crack [25]

this combination preserves the dislocation, and the size of the Burgers vector increases in the process of sliding the boundary of the grain [25].

If the value of the Burgers vector **b** of the dislocation is large enough, nanocracks appear in the stress field of the dislocation (Fig. 7, *b*). As shown in Ref. [25], in uneven blunt cracks, the stresses near the crack peak are large enough to form a nanocrack and small enough to cause dislocations with the Burgers vector. This is due to the fact that the growth of the blunt crack occurs at a relatively low stress level, which is not sufficient for the formation of dislocations with the Burgers vector. At the same time, the situation may change if the crack is blunt as a result of cage dislocations from the top of the crack or the previous emission of the grain border sliding on this peak. The stress required for the crack to grow is relatively high. For this reason, the local (local) stresses near the peak of the blunt crack may be significantly higher than the stresses near the blunt crack of the same length. Therefore, in the future, we will analyse the formation of nanocracks on the disloca-

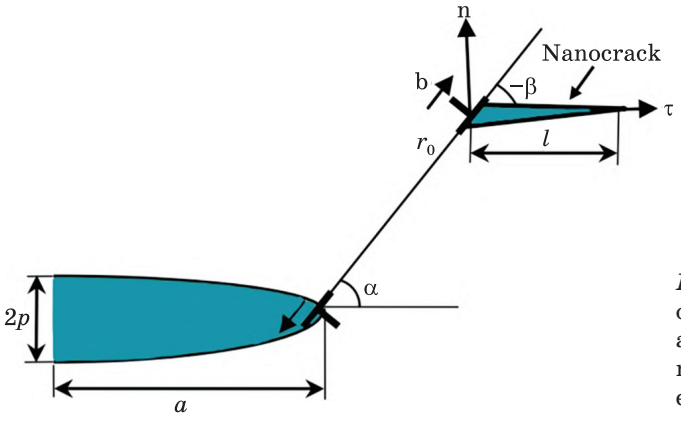

Fig. 8. Geometric view of a nanocrack formed as a result of dislocation near the apex of a long elliptical crack [25]

tion caused by the formation of the grain boundary as a result of landslides at the junction of the grain boundaries near the apex of the condensed crack (Fig. 8 [25]).

Figure 8 models a blunt roof in the form of an elongated ellipse with a radius of curvature ρ of the tip of the crack, which is smaller than the major semicircle a of the ellipse formed in the hybrid FML nanocomposites.

The radius of curvature of the ρ crack is related to a and p, the half-axes of the ellipse, with $\rho = p^2/a$ [25–27]. We model the fragmented nanocrystalline material with a modulus G and Poisson ratio ν as an elastic isotropic medium.

Let us now consider the grain boundary sliding near the apex of the condensed crack, causing dislocation with the Burgers **b** vector in hybrid FML nanocomposite compounds. Let us assume that the grain boundary, where the landslide occurs, is at an angle α to the crack plane (Fig. 8). In this case, the elliptical crack has a finite length, and the grain boundary sliding along the boundary of grain AB creates two dislocations that form a dislocation dipole (Fig. 7, *b*).

This dipole consists of the Burgers vector **b** dislocation formed by dislocation with the Burgers vector **b** located in the hybrid FML nanocomposite compound and inside the crack (Fig. 8). In fact, the formation of the second dislocation has an elliptical rift. At equilibrium, the value of the Burgers vector **b** of the dislocation dipole corresponds to the minimum energy ΔW associated with the formation of the dipole. In other words, the equilibrium value of the Burgers vector $\mathbf{b}_c$ is determined by the relation $\partial(\Delta W)/\partial b|_{b=b_c} = 0$.

In this case, the energy ΔW is determined by the expression

$$\Delta W = W_s + W_c - A, \tag{1}$$

where W_s is the specific elastic energy of the dislocation dipole, W_c is the energy of dislocation with the Burgers vector **b**, and A is the work of the displacement stress generated by the external load based on the formation of the dislocation dipole.

The specific elastic energy of the dislocation dipole reads as [27]

$$W_c = -\frac{b}{2}\int_0^{r_0 - r_c} \sigma_{r\theta}^{dip}\left(r, \theta = \alpha\right) dr\,, \tag{2}$$

where $r_c \approx b$ is the radius of the dislocation nucleus and $\sigma_{r\theta}^{dip}$, the peak of the crack, which is the beginning of the stress tensor $(0, 0)$ in the cylindrical coordinate system (r, θ) formed by the dislocation, forms a dislocation dipole of a solid with an elliptical crack (Fig. 9).

The second limit W_c is determined by the relation $W_c \approx Db^2/2$, where $D = G/(2\pi(1 - \nu))$ [28]. Finally, the final limit in Eq. (1) is calculated by the following expression [29]:

$$A = b\int_0^{r_0} \sigma_{r\theta}^{e}\left(r, \theta = \alpha\right) dr\,, \tag{3}$$

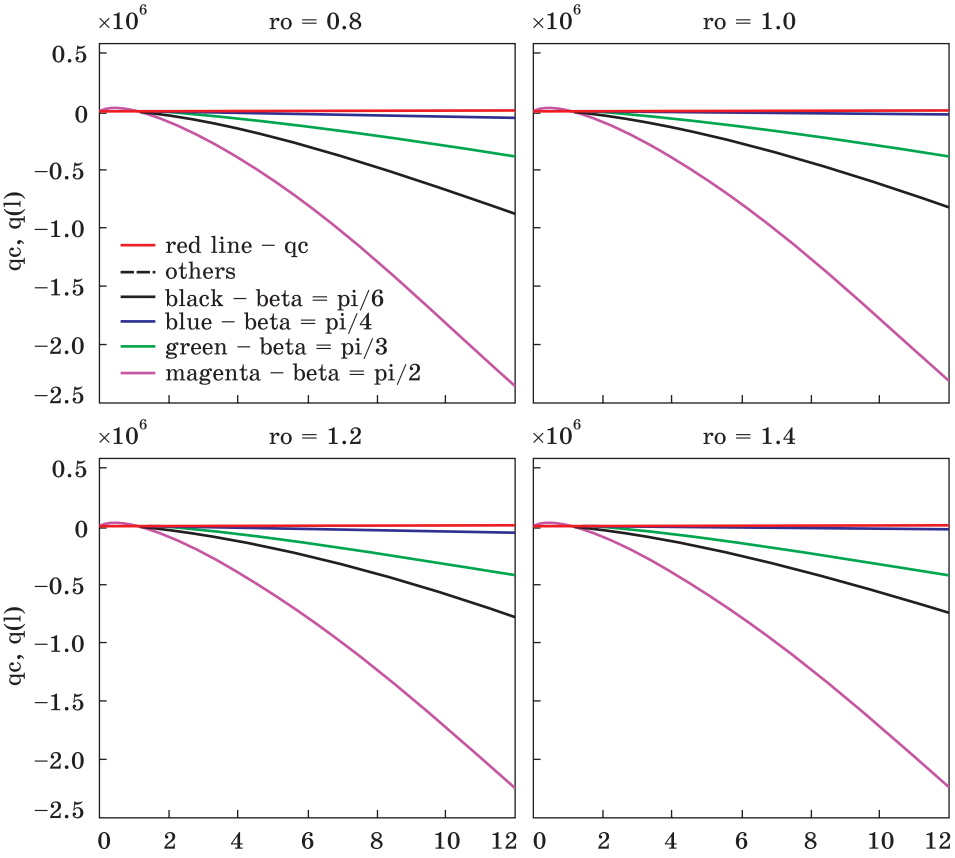

Fig. 9. The dependence of the external force on the length of nanocrack formed in the 7075-T6 aluminium matrix SiO_2 filled hybrid FML nanocomposite (colour curves online)

where $\sigma^e_{r\theta}$ are the components of the tensile tensor that generates the external mechanical load σ_0 near the peak of the elliptical crack.

The equilibrium value of the Burgers vector modulus b is calculated using Eqs. (1)–(3) applying the condition $\partial(\Delta W)/\partial b|_{b=b_c} = 0$. As a result, we get the following expression [30]:

$$b_c = \left(\frac{\sigma_0}{D}\right) f(r_0, \rho, \alpha),$$

where

$$f(r_0, \rho, \alpha) = \frac{\int_0^{r_0} \overline{\sigma}^e_{r\theta}(r, \theta = \alpha)\, dr}{1 - \int_0^{r_0 - r_c} \overline{\sigma}^{dip}_{r\theta}(r, \theta = \alpha)\, dr}. \qquad (4)$$

Now, let us calculate the external stress σ_0 required to form the dislocation dipole (Fig. 8) with the modulus b_c of the Burgers vector.

If the total tensile stress σ_p, *i.e.*, $\sigma_{yy} = \sigma_p$, around the crack peak reaches a critical value, the elliptical crack growth can be assumed [30]. The equation $\sigma_{yy} = \sigma_p$ is true when the external stress σ_0 reaches a maximum value of σ_{0_c}. Thus, the equation under study is true, when the radius of the peak of the crack ρ sometimes exceeds the critical size ρ_c.

If the critical radius is given in the form $\rho_c = 16G\gamma/(\pi\sigma_p^2(1 - \nu))$, where γ is a specific energy of the free surface [31], this value for the aluminium material will be approximately 1.4 nm.

At the tip of the crack, the stress σ_{yy} is the sum of the stress σ_{yy}^e determined by the external load and the stress σ_{yy}^{dip} generated by the dislocation dipole. Mathematically, $\sigma_{yy} = \sigma_{yy}^e + \sigma_{yy}^{dip}$. The expression for the stress σ_{yy}^e is [30]

$$\sigma_{yy}^e(x = a,\ y = 0) = 2\sigma_0\sqrt{\frac{a}{\rho}}\,. \tag{5}$$

Substituting Eq. (5) and the relation $\sigma_{yy} = \sigma_{yy}^e + \sigma_{yy}^{dip}$ into the formula $\sigma_{yy} = \sigma_p\big|_{\sigma_0=\sigma_{0c}}$ gives the expression for the maximum value of the external stress σ_{0_c} [30],

$$\sigma_0 = \frac{\sigma_p - Dbg(r_0, \alpha, \rho)}{2}\sqrt{\frac{\rho}{a}}\,, \tag{6}$$

where the function $g(r_0, \rho, \alpha)$ is given through the following relation: $\sigma_{yy}^{dip} = Db\overline{\sigma}_{yy}^{dip} = Dbg(r_0, \rho, \alpha)$.

In the case of $b = b_c$ and $\sigma_0 = \sigma_{0_c}$, after substituting the expression $b_c = (\sigma_c/D)f(r_c, \rho, \alpha)$ into Eq. (6) and solving the final equation for σ_{0_c}, we obtain the following expression:

$$\sigma_{0c} = \frac{\sigma_p}{2\sqrt{a/\rho} + f(r_0, \rho, \alpha)g(r_0, \rho, \alpha)}\,, \tag{7a}$$

$$b_c = \frac{\sigma_p}{D}\frac{f(r_0, \rho, \alpha)}{2\sqrt{a/\rho} + f(r_0, \rho, \alpha)g(r_0, \rho, \alpha)}\,. \tag{7b}$$

The functions $f(r_0, \rho, \alpha)$ and $g(r_0, \rho, \alpha)$ depend on the stresses $\sigma_{r\theta}^e$, $\sigma_{r\theta}^{dip}$ and σ_{yy}^{dip} created by the external load σ_0 and the dislocation dipole in an infinite elastic medium with an elliptical crack [32]. From the scientific work, we find the following expressions for these tensions. The stress $\sigma_{r\theta}^e$ generated by the elliptical crack in an infinite elastic medium σ_0 is given mathematically as follows [33]:

$$\sigma_{r\theta}^e = \mathrm{Im}\left[\left(\overline{z}\varphi_e''(z) + \psi_e'(z)\right)e^{2i\theta}\right],\ z = x + iy = a + re^{i\theta},\ i = \sqrt{-1}\,. \tag{8}$$

The functions $\varphi_e(x)$ and $\psi_e(z)$ in Eq. (8) are complex variable potentials defined by the following equations [34]:

$$\varphi_e(x) = \frac{\sigma_0 R}{4}\left(\xi - (2 + m)\frac{1}{\xi}\right), \tag{9a}$$

$$\psi_e(x) = \frac{\sigma_0 R}{2}\left(\xi - \frac{1}{\xi} - \frac{(1+m)(1+m\xi^2)}{\xi(\xi^2 - m)}\right), \tag{9b}$$

where

$$R = \sqrt{a}\,\frac{\sqrt{a}+\sqrt{\rho}}{2}, \quad m = \frac{\sqrt{a}-\sqrt{\rho}}{\sqrt{a}+\sqrt{\rho}},$$

and ξ is one of the two roots of equation $z = R(\xi + m/\xi)$ within the condition $|\xi| \geq 1$.

The stress field $\sigma_{ij}^{dip}(r,\theta)$ generated by the dislocation dipole in an infinite elastic medium with an elliptical crack (Figs. 7 and 8) is calculated from the ratio $\sigma_{ij}^{dip}(r,\theta) = \sigma_{ij}^{d}(r_0,\alpha,\theta,r) - \sigma_{ij}^{d}(0,\alpha,\theta,r)$, where $\sigma_{ij}^{d}(r_0,\alpha,\theta,r)$ is the stress field resulting from the dislocation at point B (Fig. 7, *b*), and $\sigma_{ij}^{d}(0,\alpha,\theta,r)$ is the stress field resulting from the dislocation located inside the elliptical crack (Fig. 7, *b*).

The stress $\sigma_{ij}^{d}(r_0,\alpha,\theta,r)$ is calculated from the following relation [2, 31, 32]:

$$\sigma_{r\theta}^{d}(r_0,\alpha,\theta,r) = \mathrm{Im}\left[\left(\bar{z}\varphi_d''(z) + \psi_d'(z)\right)e^{2i\theta}\right], \tag{10}$$

where

$$\varphi_d(z) = A\ln(z - z_d) + \varphi_{im}(z), \tag{11a}$$

$$\psi_d(z) = \bar{A}\ln(z - z_d) - A\frac{\bar{z}_d}{(z - z_d)} + \psi_{im}(z), \tag{11b}$$

$$\begin{aligned}\varphi_{im}(z) = {} & 2A\ln\xi - A\ln\left(\xi - \frac{m}{\xi_d}\right) - A\ln\left(\xi - \frac{1}{\bar{\xi}_d}\right) + \\ & + \bar{A}\,\frac{\xi_d(1 + m\bar{\xi}_d^2) - \bar{\xi}_d(\xi_d^2 + m)}{\xi_d\bar{\xi}_d(\bar{\xi}_d^2 - m)(\xi - 1/\bar{\xi}_d)},\end{aligned} \tag{12}$$

$$\begin{aligned}\psi_{im}(z) = {} & 2\bar{A}\ln\xi - \bar{A}\ln\left(\xi - \frac{m}{\xi_d}\right) - \bar{A}\ln\left(\xi - \frac{1}{\bar{\xi}_d}\right) + \\ & + A\,\frac{\bar{\xi}_d(\xi_d^2 + m^3) - m\xi_d(\bar{\xi}_d^2 + m)}{\xi_d\bar{\xi}_d\left(\bar{\xi}_d^2 - m\right)\left(\xi - m/\xi_d\right)} - \xi\,\frac{1 + m\xi^2}{\xi^2 - m}\,\frac{d\varphi_{im}}{d\xi};\end{aligned} \tag{13}$$

here, ξ_d is one of the root of the equation $z_d = R(\xi_d + m/\xi_d)$, such that $|\xi_d| \geq 1$, $z = a + r_0 e^{i\theta}$, $z_d = a + re^{i\theta}$, and $A = Gbe^{i\theta}/(4\pi(1-\nu))$.

Similar to Eq. (10), the expressions for the stress tensor components σ_{yy}^{d}, σ_{nn}^{d}, and $\sigma_{\tau n}^{d}$ [1, 2, 31, 32] are as follow:

$$\sigma_{yy}^{d}(r_0,\alpha,\theta,r) = \mathrm{Im}\left[2\varphi_d(z) + \bar{z}\varphi_d''(z) + \psi_d'(z)\right], \tag{14}$$

$$\sigma_{nn}^{d}(r_0,\alpha,\theta,r) = \mathrm{Im}\left[\left(2\varphi_d'(z) + \bar{z}\varphi_d''(z) + \psi_d'(z)\right)e^{2i(\alpha+\beta)}\right], \tag{15}$$

$$\sigma_{\tau n}^{d}(r_0,\alpha,\theta,r) = \mathrm{Im}\left[\left(\bar{z}\varphi_d'(z) + \psi_d'(z)\right)e^{2i(\alpha+\beta)}\right]. \tag{16}$$

The expressions for the stresses $\sigma_{r\theta}^{dip}$, σ_{yy}^{dip}, σ_{nn}^{dip}, $\sigma_{\tau n}^{dip}$ can be obtained from Eqs. (10)–(16) and relation $\sigma_{ij}^{dip}(r,\theta) = \sigma_{ij}^{d}(r_0,\alpha,\theta,r) - \sigma_{ij}^{d}(0,\alpha,\theta,r)$. The functions $f(r_0,\alpha,\rho)$ and $g(r_0,\alpha,\rho)$ can be calculated from the above expressions, Eq. (4), and expression $g(r_0,\alpha,\rho) = \sigma_{yy}^{dip}/Db$.

Let us consider now the conditions for the formation and growth of a nanocrack on a dislocation in a hybrid FML nanocomposite compound near the apex of an elliptical crack (Figs. 7 and 8). Assume that the length of the nanocrack is l, and the angle β is in the plane of the grain boundary where the grain boundary slip occurs. In the first approximation, we will consider the growth of nanocracks in the stress field created by the dislocation dipole between the nanocrack and the elliptical crack, and the load applied to the composite by the elliptical cracks. When we consider the growth of nanocracks, we will model it as a diffuse crack in an infinite body affected by a stress field. Thus, we will ignore the effect of the additional stress field created by the formation and growth of large elliptical nanocracks.

We will use the next growth criterion of nanocrack to calculate the growth conditions of nanocracks [35]:

$$F > 2\gamma_e, \tag{17}$$

where F is the configuration force, if the nanocrack grows within the grain; then, $\gamma_e = \gamma$, if the nanocrack grows along the grain boundary; then, $\gamma_e = \gamma - \gamma_b/2$ where γ_b is the specific energy of the grain boundary. The configuration force in the approximation used is calculated by the following equation [35].

$$F = \frac{\pi l(1-\nu)}{4G}(\bar{\sigma}_{nn}^2 + \bar{\sigma}_{\tau n}^2), \tag{18}$$

where τ is the vector directed to the dislocation line along the nanocrack, n is the normally directed vector to the nanocrack (Fig. 8), σ_{nn} and $\sigma_{\tau n}$ are the components of the dislocation dipole of the solid with elliptical crack and the field of stresses created by external load, $\bar{\sigma}_{nn}$ and $\bar{\sigma}_{\tau n}$ are the average weight values of these stresses. The quantities $\bar{\sigma}_{nn}$ and $\bar{\sigma}_{\tau n}$ are determined by the following relations [35]:

$$\bar{\sigma}_{kn} = \frac{2}{\pi l}\int_0^l \sigma_{kn}\sqrt{\frac{\tau}{l-\tau}}d\tau\,,\ k = n,\ \tau. \tag{19}$$

In addition to fulfilling Eq. (18) for the growth of the nanocrack, we will require that the stress in the formation of the nanocrack be positive in the plane of the nanocrack. Considering Eq. (19) in the Eq. (18), we rewrite the growth of the nanocrack under the condition $q > q_c$ and here we get the expressions $q = (\pi l/2)(\bar{\sigma}_{nn}^2 + \bar{\sigma}_{\tau n}^2)$ and $q_c = 4\pi/G(1-\nu)$. The growth of nanoparticles in 7075-T6 aluminium matrix SiO_2 and clay filler hybrid FML nanocomposites was calculated using Eqs. (18) and (19) based on the two sets of parameters:

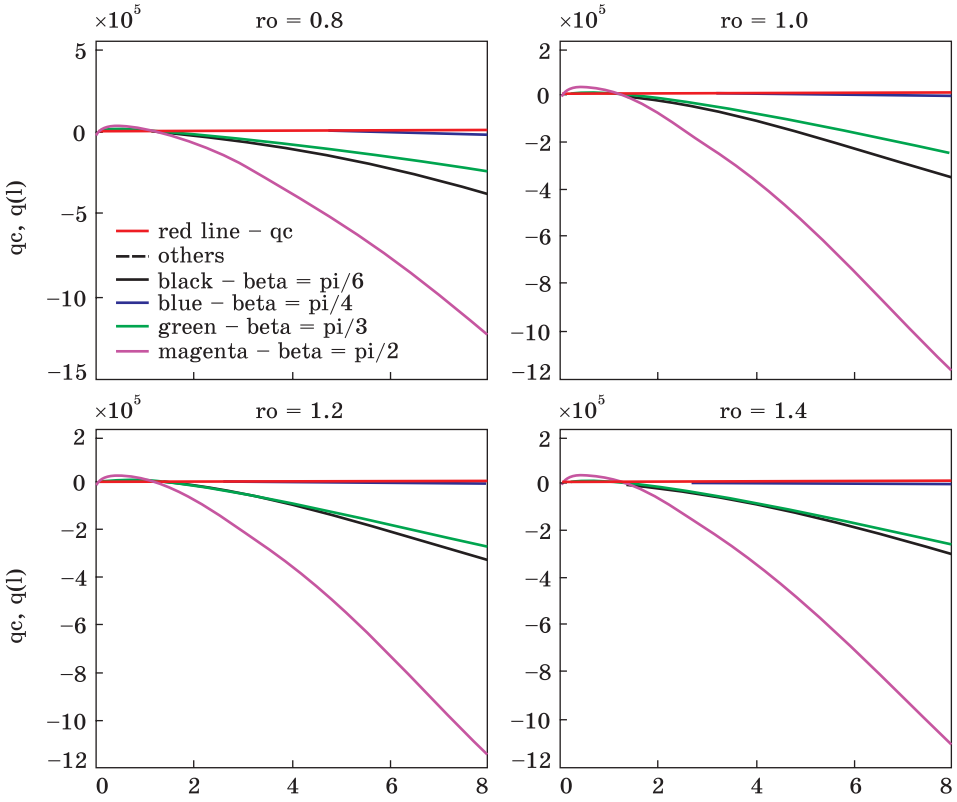

Fig. 10. The dependence of the external force on the length of nanocrack formed in the 7075-T6 aluminium matrix clay filled hybrid FML nanocomposite (colour curves online)

(1) σ_p = 28.8 MPa, γ = 1.41 J/m^2, ν = 0.132, G = 58 MPa, a = 1 μm, $\alpha = \pi/3$, $\beta = \pi/2, \pi/4, 0, \pi$; ρ = 0.8, 1.0, 1.2, 1.4;

(2) σ_p = 28.8 MPa, γ = 1.18 J/m^2, ν = 0.272, G = 42 MPa, a = 2.5 μm, $\alpha = \pi/3$, $\beta = \pi/2, \pi/4, 0, \pi$; ρ = 0.8, 1.0, 1.2, 1.4.

The $q(l)$ dependences are described in Fig. 9 for the 7075-T6 aluminium matrix SiO_2-filled hybrid FML nanocrystalline state at r_0 = 10 nm and at different values of ρ and β. In this way, the horizontal lines show the values of q_c. The growth of the nanocrack is favourable in terms of energy in the regions where $q(l)$ located above the horizontal line $q = q_c$. As can be seen from Fig. 9, the conditions for the formation and growth of nanocracks in nanocrystalline materials are determined by the increase in the radius of curvature of the ρ-peak.

In addition to the radius of curvature of the crack peak, ρ is an important parameter that affects the formation and growth of nanocracks; r_0 is the distance from the junction of the grain boundary to the dislocation at the apex of the blunt crack.

In Figure 10, the clay filler hybrid with 7075-T6 aluminium matrix shows different values of $q(l)$ curves $\beta = \pi/2$ for the FML nanocrystalline state and r_0. As can be seen from Fig. 10, a fairly large increase in r_0 makes it difficult to form nanocracks longer than a few nanometres in length. The reason for this is that as r_0 increases, the stress created by the load applied to the nanocrack plane decreases. This decrease in the stresses created by the applied load has a great effect on the growth of the nanocracks, not only on the increase of r_0, but also on the growth of the Burgers vector.

It should be noted that r_0 is the length of the grain boundary or part of it (Fig. 7). Therefore, the decrease in r_0 moderates with decreasing grain size. In this case, since the decrease in r_0 facilitates the formation of nanocracks (Fig. 10), the growth processes of their formation near blunt cracks are more likely in nanocrack materials with a decrease in grain size.

Thus, the following is shown within the model. First, the conditions for the formation and growth of nanocracks in nanocrystalline materials become easier with increasing radius of curvature ρ (Fig. 9) that means that blunt cracks do not effectively affect the fragility of nanocrystalline materials. As a rule, it is a micromechanism associated with a high degree of plasticity and viscosity in traditional polycrystalline metals. On the other hand, the formation and growth of nanocracks in nanocrystalline materials becomes more pronounced with a decrease in the size of the grains (Fig. 10). In other words, reducing the grain size reduces the plasticity of nanocrystalline materials.

4. Discussion

Experimental data on the formation of cracks in hybrid nanocrystalline materials with nanoparticle filler 7075-T6 aluminium matrix under the influence of high-velocity and quasi-static deformation regimes, the results of computer and theoretical model reviews were compared with the results of literature studies.

Typical elemental cracks in nanocrystalline materials are nanocracks formed at the grain boundaries and compounds in the areas of dislocation stresses caused by intergranular sliding (Fig. 6). Elliptic cracks (Fig. 8) are typical carriers of the disintegration process. In nanocrystalline and nanocomposite materials, cracks often form and grow along curved grain boundaries [36, 37]. The formation of typical nanocracks under mechanical load determines the mechanism of disintegration acting on nanocrystalline materials [37]. First of all, it depends on the size of the grain, its structural properties, material parameters and loading conditions [38], and occurs along high-grained nanocrystalline metallic materials along plastic grain flows. In this case, due to the limited plas-

tic displacement at the joints of the grain boundaries, such joints are a source of high local stresses [39–41]. Relaxation of these local stresses, the formation of nanocracks at 4/3 of the grain boundaries is carried out effectively (Fig. 6) [20]. This process is intensified during quasi-static deformation near the peaks of microcracks in nanocrystalline materials. Also, the formation of nanocracks in three-layer joints of grain boundaries is effectively carried out under the influence of ultra-high stresses during high-speed deformation [36, 37, 42]. Nanocrystalline materials (including quasi-two-dimensional ones [43, 44]) exhibit special behaviour when subjected to high-speed deformation. In this case, the main microstructural features of nanocrystalline 7075-T6 aluminium matrix hybrid FML samples after impact after high-speed deformation are the preservation of the initial nanocrystalline state with the initial values of average grain size and high density of lattice dislocations [28]. The results of modelling the molecular dynamics of nanocrystalline aluminium behaviour under impact loading [45, 46] show the effect of plastic deformation of the grain boundary and cage sliding modes on the shock front (Fig. 6). In the work on modelling the molecular dynamics of impact loading of nanocrystalline materials [42], abnormally high values of its strength were found in the area behind the impact front (Fig. 5).

5. Conclusions

In this article, experimental and theoretical results obtained from hybrid FML nanocrystal composite materials are analysed based on computer modelling.

The proposed model explains the experimental observations of nanocracks in the combinations of grain boundaries of hybrid nanocomposites close to the peaks of blunt cracks during loading. Cracks formed in nanocrystalline materials are nanocracks formed at the borders of grains. In hybrid FML nanocrystalline composites, nanocracks have been found to form at the junctions of grain boundaries before the peaks of large cracks. The formation and growth of nanocracks in nanocrystalline materials is explained by the reduction in grain size. In other words, a reduction in grain size reduces the plasticity of the nanocrystalline material. The results are consistent with experimental data on the low viscosity and plasticity of most nanocrystalline materials. In addition, in some nanocrystalline metals, the reduction in grain size corresponds to the viscous-brittle transition observed experimentally. The obtained results confirm the experimental results on the low viscosity and plasticity of most nanocrystalline materials.

REFERENCES

1. H. Conrad and J. Narayan, *Appl. Phys. Lett.*, **81**, No. 12: 2241 (2002); https://doi.org/10.1063/1.1507353
2. M.J. Demkowicz, A.S. Argon, D. Farkas, and M. Frary, *Philos. Magaz.*, **87**, No. 28: 4253 (2007); https://doi.org/10.1080/14786430701358715
3. M.Yu. Gutkin and I.A. Ovid'ko, *Phys. Solid State*, **52**: 1397 (2010); https://doi.org/10.1134/S1063783410070127
4. J.N. Aslanov and A.B. Sultanova, *IFAC-PapersOnLine*, **51**, No. 30: 12 (2018); https://doi.org/10.1016/j.ifacol.2018.11.236
5. H.A. Padilla and B.L. Boyce, *Exp. Mech.*, **50**: 5 (2010); https://doi.org/10.1007/s11340-009-9301-2
6. I. Hasanov, I. Abbasov, and N. Gurbanov, *Proc. Latvian Acad. Sci. Sec. B*, **74**, No. 4: 727 (2020); https://doi.org/10.2478/prolas-2020-0044
7. K.A. Padmanabhan and H. Gleiter, *Mater. Sci. Eng. A*, **381**, Nos. 1–2: 28 **(**2004); https://doi.org/10.1016/j.msea.2004.02.054
8. N.A. Gurbanov and M.B. Babanli, *Metallofiz. Noveishie Tekhnol.*, **43**, No. 12: 1589 (2021); https://doi.org/10.15407/mfint.43.12.1589
9. D. Farkas, H. Van Swygenhoven, and P.M. Derlet, *Phys. Rev. B*, **66**, No. 6: 060101 (2002); https://doi.org/10.1103/PhysRevB.66.060101
10. T. Hanlon, Y.-N. Kwon, and S. Suresh, *Scr. Mater.*, **49**, No. 7: 675 (2003); https://doi.org/10.1016/S1359-6462(03)00393-2
11. A. Latapie and D. Farkas, *Phys. Rev. B*, **69**, No. 13: 134110 (2004); https://doi.org/10.1103/PhysRevB.69.134110
12. I.A. Ovid'ko and A.G. Sheinerman, *Acta Mater.*, **52**, No. 5: 1201 (2004); https://doi.org/10.1016/j.actamat.2003.11.004
13. I.A. Ovid'ko and A.G. Sheinerman, *Phys. Rev. B*, **77**, No. 5: 054109 (2008); https://doi.org/10.1103/PhysRevB.77.054109
14. J.N. Aslanov, V.T. Mamedov, and G.A. Mamedov, *J. Appl. Mech. Tech. Phys.*, **61**: 286 (2020); https://doi.org/10.1134/S0021894420020157
15. I.A. Ovid'ko and A.G. Sheinerman, *Phys. Solid State*, **50**: 1044 (2008); https://doi.org/10.1134/S1063783408060085
16. I.A. Ovid'ko and A.G. Sheinerman, *Acta Mater.*, **57**, No. 7: 2217 (2009); https://doi.org/10.1016/j.actamat.2009.01.030
17. D. Farkas, S. Petegem, P.M. Derlet, and H. Van Swygenhoven, *Acta Mater.*, **53**, No. 11: 3115 (2005); https://doi.org/10.1016/J.ACTAMAT.2005.02.012
18. D. Wolf, V. Yamakov, S.R. Phillpot, A.K. Mukherjee, and H. Gleiter, *Acta Mater.*, **53**, No. 1: 1 (2005); https://doi.org/10.1016/j.actamat.2004.08.045
19. M.A. Vasylyev, S.M. Voloshko, V.I. Zakiev, A.P. Burmak, Ya.I. Matvienko, and A.D. Rud, *Metallofiz. Noveishie Tekhnol.*, **43**, No. 11: 1455 (2021); https://doi.org/10.15407/mfint.43.11.1455
20. N.A. Gurbanov, M.Y. Askin, M.B. Babanli, and Y. Turen, *Funct. Mater.*, **29**, No. 1: 172 (2022); https://doi.org/10.15407/fm29.01.172

21. A. Afrouzian, H.M. Aleni, G.H. Liaghat, and H. Ahmadi, *J. Reinforced Plastics and Composites*, **36**, No. 12: 900 (2017); https://doi.org/10.1177/0731684417694753
22. K.S. Kumar, S. Suresh, M.F. Chisholm, J.A. Horton, and P. Wang, *Acta Mater.*, **51**, No. 2: 387 (2003); https://doi.org/10.1016/S1359-6454(02)00421-4
23. K.S. Kumar, H. Van Swygenhoven, and S. Suresh, *Acta Mater.*, **51**, No. 19: 5743 (2003); https://doi.org/10.1016/j.actamat.2003.08.032
24. S.V. Bobylev, A.K. Mukherjee, I.A. Ovid'ko, and A.G. Sheinerman, *Int. J. Plasticity*, **26**, No. 11: 1629 (2010); https://doi.org/10.1016/j.ijplas.2010.03.001
25. I.A. Ovid'ko and A.G. Sheinerman, *J. Phys. D: Appl. Phys.*, **46**, No. 34: 345305 (2013); https://doi.org/10.1088/0022-3727/46/34/345305
26. S.P. Repetsky, E.G. Len, and V.V. Lizunov, *Metallofiz. Noveishie Tekhnol.*, **28**, No. 8: 989 (2006).
27. T. Mura, *Micromechanics of Defects in Solids* (Dordrecht: Springer–Kluwer Academic Publishers: 1987); https://doi.org/10.1007/978-94-009-3489-4
28. Z. Zhuang, Z. Liu, and Y. Cui, *Dislocation Mechanism-Based Crystal Plasticity: Theory and Computation at the Micron and Submicron Scale* (Academic Press: 2019).
29. L.L. Fischer and G.E. Beltz, *J. Mech. Phys. Solids*, **49**, No. 3: 635 (2001); https://doi.org/10.1016/S0022-5096(00)00042-9
30. G.E. Beltz, D.M. Lipkin, and L.L. Fischer, *Phys. Rev. Lett.*, **82**, No. 22: 4468 (1999); https://doi.org/10.1103/PhysRevLett.82.4468
31. I.A. Ovid'ko and A.G. Sheinerman, *Acta Mater.*, **58**, No. 16: 5286 (2010); https://doi.org/10.1016/j.actamat.2010.05.058
32. M.Yu. Gutkin and I.A. Ovid'ko, *Plastic Deformation in Nanocrystalline Materials* (Springer: 2004).
33. R.K. Mehtiyev, *Proc. 7th International Conf. Control and Optimization with Industrial Applications Pace (August 26–28, 2020, Baku, Azerbaijan)* (COIA: 2020), p. 269.
34. R.K. Mehtiyev, *Proc. 6th International Conf. Control and Optimization with Industrial Applications Pace (July 11–13, 2018, Baku, Azerbaijan)* (COIA: 2020), p. 223.
35. D.M. Hulbert, D. Jiang, J.D. Kuntz, Y. Kodera, and A.K. Mukherjee, *Scr. Mater.*, **56**, No. 12: 1103 (2007); https://doi.org/10.1016/j.scriptamat.2007.02.003
36. I.A. Ovid'ko and A.G. Sheinerman, *Acta Mater.*, **53**, No. 5: 1347 (2005); https://doi.org/10.1016/j.actamat.2004.11.026
37. J. Wan, R.-G. Duan, M.J. Gasch and A.K. Mukherjee, *J. Amer. Ceram. Soc.*, **89**, No. 1: 274 (2006); https://doi.org/10.1111/j.1551-2916.2005.00702.x
38. T.G. Jabbarov, O.A. Dyshin, M.B. Babanli, and I.I. Abbasov, Mathematical modelling of the sintering process of iron-based metal-glass materials, *Prog. Phys. Met.*, **20**, No. 4: 584 (2019); https://doi.org/10.15407/ufm.20.04.584
39. X. Mao, L. Qiao, and X. Li, *Scr. Mater.*, **39**, Nos. 4–5: 519 (1998); https://doi.org/10.1016/s1359-6462(98)00191-2
40. X. Li and X. Jiang, *Eng. Fract. Mech.*, **211**: 258 (2019); https://doi.org/10.1016/j.engfracmech.2019.03.038

41. E. Zolgharnein and V.M. Mirsalimov, *Acta Polytechnica Hungarica*, **9**, No. 2: 169 (2012).
42. G.-D. Zhan, J.D. Kuntz, J. Wan, and A.K. Mukherjee, *Nature Mater.*, **2**: 38 (2003); https://doi.org/10.1038/nmat793
43. A.G. Solomenko, R.M. Balabai, T.M. Radchenko, and V.A. Tatarenko, Functionalization of quasi-two-dimensional materials: chemical and strain-induced modifications, *Prog. Phys. Met.*, **23**, No. 2: 147 (2022); https://doi.org/10.15407/ufm.23.02.147
44. V.V. Girzhon and O.V. Smolyakov, Modelling of lattices of two-dimensional quasi-crystals, *Prog. Phys. Met.*, **20**, No. 4: 551 (2019); https://doi.org/10.15407/ufm.20.04.551
45. V.M. Mirsalimov and Sh.G. Hasanov, *Int. J. Damage Mech.*, **23**, No. 3: 430 (2014); https://doi.org/10.1177/1056789513519459
46. N.J.M. Carvalho, B.J. Kooi, and J.Th.M. De Hosson, *Surface Treatment VI: Computer Methods and Experimental Measurements for Surface Treatment Effects.* (Southampton, NY: WIT Press: 2002), p. 233.

Received 10.01.2022;
in final version, 21.06.2022

М.В. Бабанли, Н.А. Гурбанов, Р.К. Мехтієв
Азербайджанський державний університет нафти та промисловости,
просп. Азадлиґ, 20, 1010 Баку, Азербайджан

УТВОРЕННЯ ТА РІСТ ТРІЩИН У ГІБРИДНИХ ВОЛОКНИСТИХ МЕТАЛЕВИХ ЛАМІНАТНИХ НАНОКОМПОЗИТНИХ МАТЕРІАЛАХ ІЗ АЛЮМІНІЙОВОЮ МАТРИЦЕЮ 7075-Т6

Роботу сфокусовано на експериментальних даних, комп'ютерних і теоретичних (аналітичних) моделях процесів утворення тріщин у гібридних нанокристалічних матеріалах з алюмінійовою матрицею 7075-Т6 і наночастинковим наповнювачем під впливом високошвидкісних і квазистатичних режимів деформації. Із наведенням основних експериментальних фактів та результатів комп'ютерного моделювання особливу увагу приділено теоретичним моделям, що описують утворення наноскопічних тріщин на вершинах мікротріщин у гібридних нанокристалічних матеріалах за високих швидкостей і квазистатичних деформацій. Запропоновано модель, що описує утворення та зростання нанотріщин біля вершин затуплених тріщин у гібридному нанокомпозитному матеріалі. В межах моделі концентрація напружень на вершині затуплених тріщин зумовлює ковзання меж зерен і дислокації в стиках меж зерен. Напруження, що створюють ці дислокації, і навантаження, прикладене до піків тріщин, спричинюють утворення та зростання нанотріщин. Показано, що збільшення радіуса кривини на вершині товстої тріщини та зменшення розміру зерен сприяють зростанню нанотріщин. Ці тенденції узгоджуються з експериментальними даними щодо низької в'язкости розпаду та високої пластичности більшости нанокристалічних матеріалів.

Ключові слова: волокнистий металевий ламінат (ВМЛ), гібридний ВМЛ нанокомпозит, еліптична тріщина, в'язке розтріскування, розтягання, пластичність.